Application of turbulence models to equilibrium boundary layers under adverse pressure gradient

By Ruud A. W. M. Henkes [*], Martin Skote[†] and Dan S. Henningson[†‡]

Four classes of turbulence models (algebraic, $k-\epsilon$, $k-\omega$ and a differential Reynolds-stress model) are applied to boundary layers under adverse pressure gradient with a constant equilibrium parameter $\beta = \frac{\delta^*}{\tau_w}\frac{dp}{dx}$. Numerical solutions up to $Re_\theta = 10^8$ give the classical scalings in the inner and outer layer for all models. Comparison is made with experiments of Clauser at $\beta \approx 2$ and 8 and with recent experiments by Skåre and Krogstad at $\beta = 20$. We have also performed new direct numerical simulations at $\beta \approx 0.25$ and 0.65 up to $Re_\theta = 700$. The differential Reynolds-stress model shows the best agreement with the experiments and the DNS.

1. Introduction

The present study considers the scalings according to four commonly used turbulence models for equilibrium boundary layers under an adverse pressure gradient. According to Clauser (1954), the boundary layer is in equilibrium if the parameter $\beta = \frac{\delta^*}{\tau_w}\frac{dp}{dx}$ is independent of the streamwise position. The scalings are derived from the turbulence models without making any additional a priori assumptions, which means that the scalings follow from the straightforward numerical solution of the boundary-layer equations. Computations are made up to the very large Reynolds number of $Re_\theta \approx 10^8$, which is sufficient for the similarity scalings to appear. A strong grid refinement was applied close to the wall. By doubling the number of grid points, the solutions were verified to be numerically accurate.

The classical theory, which is mainly due to Clauser (1954) and Coles (1956), finds that the boundary layer can be split up in an inner layer (wall

[*]Faculty of Aerospace Engineering, Delft University of Technology, Kluyverweg 1, 2629 HS Delft, The Netherlands. Present address: Shell Research and Technology Centre Amsterdam, P.O. Box 3003, 1003 AA Amsterdam, The Netherlands

[†]Department of Mechanics, Royal Institute of Technology (KTH), SE-100 44 Stockholm, Sweden

[‡]Aeronautical Research Institute of Sweden (FFA), Box 11021, SE-161 11 Bromma, Sweden

function), with length scale ν/u_τ and velocity scale u_τ, and an outer layer (defect layer), with the velocity scale u_τ and the length scale $\Delta = \delta^* U/u_\tau$ (where U denotes the local free-stream velocity).

The results for the turbulence models are compared with experiments at moderate Reynolds numbers ($Re_\theta = 10^4$ to 10^5) for $\beta \approx 2$ and 8, obtained by Clauser (1954), and with more recent experiments at $\beta = 20$, being close to separation, due to Skåre (1994) and Skåre & Krogstad (1994). Furthermore, the results with the turbulence models are also compared with new direct numerical simulations for $\beta \approx 0.25$ and 0.65 up to $Re_\theta \approx 700$, which we performed with a spectral code.

2. Scaling analysis

To derive the scalings of the boundary layer under an adverse pressure gradient one can start from the turbulent boundary-layer equations for an incompressible flow, which read

$$\frac{\partial u}{\partial x} + \frac{\partial v}{\partial y} = 0, \tag{1}$$

$$u\frac{\partial u}{\partial x} + v\frac{\partial u}{\partial y} = -\frac{1}{\rho}\frac{dp}{dx} + \nu\frac{\partial^2 u}{\partial y^2} - \frac{\partial}{\partial y}\overline{u'v'}. \tag{2}$$

Here x and y are the coordinates along and normal to the wall, respectively; u and v are the corresponding velocity components; p is the pressure; ρ is the density; ν is the kinematic viscosity; and $-\overline{u'v'}$ is the Reynolds shear stress.

According to the classical theory, the velocity scale in both the inner and outer layer is the same, namely u_τ, which is the wall-shear stress velocity $(\tau_w/\rho)^{1/2}$, with τ_w being the wall-shear stress $\mu(\partial u/\partial y)_w$. The length scale differs, and is ν/u_τ for the inner layer and $\Delta = \delta^* U/u_\tau$ for the outer layer; δ^* is the displacement thickness, and U is the local outer-edge velocity. Tennekes & Lumley (1972) and Wilcox (1993) have derived a so-called defect-layer equation, which is the equation that describes the similarity solution in the outer layer. There is, however, a striking difference between the derivations of Tennekes & Lumley and Wilcox. We have reconsidered the analysis (for more details see Henkes, 1998) and find agreement with the results by Tennekes & Lumley.

When it is assumed that molecular diffusion can be neglected in the outer layer, the boundary-layer equations (1)-(2) can be transformed into

$$(\beta - 2\omega)f + \gamma f^2 + (\alpha - 2\beta - 2\omega)\eta f' - \chi f' \int_0^\eta f\,d\eta = r', \tag{3}$$

with

$$\alpha = \left(\frac{U}{u_\tau}\right)^2 \frac{d\delta^*}{dx},\ \beta = \frac{\delta^*}{\tau_w}\frac{dp}{dx}, \tag{4}$$

$$\omega = \frac{1}{2}\frac{\delta^*}{u_\tau}\left(\frac{U}{u_\tau}\right)^2 \frac{du_\tau}{dx},$$

$$\gamma = \frac{U}{u_\tau}\frac{\delta^*}{u_\tau}\frac{du_\tau}{dx},\ \chi = \frac{U}{u_\tau}\frac{d\delta^*}{dx} + \frac{\delta^*}{u_\tau}\frac{dU}{dx}.$$

Here $\eta = y/\Delta$, $f(\eta) = \dfrac{U-u}{u_\tau}$, and $r(\eta) = -\dfrac{\overline{u'v'}}{u_\tau^2}$. A prime denotes differentiation to η.

The coefficients can be developed in a series with respect to the small quantity u_τ/U (see Henkes, 1998), which gives

$$\alpha = 1 + 3\beta + (1+\beta)C^* \frac{u_\tau}{U} + ..., \tag{5}$$

$$\omega = -\frac{1}{2}\beta - \frac{1}{2\kappa}(1+2\beta)\frac{u_\tau}{U} + ...,$$

$$\gamma = -\beta\frac{u_\tau}{U} - \frac{1}{\kappa}(1+2\beta)\left(\frac{u_\tau}{U}\right)^2 + ...,$$

$$\chi = (1+2\beta)\frac{u_\tau}{U} + ...,$$

with $C^* = \int_0^\infty f^2 d\eta$, and κ is the Von Kármán constant. To leading order eq. (5) gives

$$\alpha = 1 + 3\beta,\ \omega = -\frac{1}{2}\beta,\ \gamma = \chi = 0. \tag{6}$$

Therefore, for increasing Re_θ (giving $u_\tau/U \to 0$) equation (3) converges to the following defect-layer equation for the outer layer

$$2\beta f + (1+2\beta)\eta f' = r', \tag{7}$$

with boundary conditions

$$f \to -\frac{1}{\kappa}\ln\eta + C' \text{ for } \eta \to 0, \tag{8}$$

$$f \to 0 \text{ for } \eta \to \infty,$$

and the integral restriction

$$\int_0^\infty f d\eta = 1. \tag{9}$$

The boundary condition for $\eta \to 0$ follows from matching with the logarithmic wall function, and the integral restriction follows from the conservation of momentum. Equation (7) was also obtained by Tennekes & Lumley, but Wilcox took $\omega = 0$ (instead of $\omega = -\frac{1}{2}\beta$) and thus arrived at a different equation.

3. Turbulence models

To solve the boundary-layer equations (1) and (2) or the defect-layer equation (7), a turbulence model is needed to represent the Reynolds shear stress. The following models are considered:

- Algebraic model of Cebeci & Smith (1974)
- Two-equation low-Reynolds-number $k-\epsilon$ model of Launder & Sharma (1974)
- Two-equation low-Reynolds-number $k-\omega$ model of Wilcox (1993)
- Differential Reynolds-Stress Model (DRSM) of Hanjalić *et al.* (1995)

The algebraic model uses an algebraic relation to approximate the turbulent viscosity which appears in $-\overline{u'v'} = \nu_t \dfrac{\partial u}{\partial y}$. The $k-\epsilon$ model solves differential equations for the turbulent kinetic energy and the turbulent dissipation rate ϵ to model the turbulent viscosity, whereas the $k-\omega$ model solves a differential equation for ω instead of ϵ (where ω is proportional to ϵ/k). The DRSM is the most complete model, as it solves differential equations for all Reynolds shear and normal stresses, as well as for ϵ. More details of the models are given in the cited references, and in Henkes (1997).

The boundary-layer equations are solved with a marching numerical procedure, after discretization with a second-order finite-difference scheme. A Cartesian grid is used with a very strong grid refinement in the lower part of the inner layer. To account for the growth of the boundary layer in streamwise direction, at several x positions the outer edge was increased and the y grid points were redistributed. All results presented in this paper are guaranteed to be grid independent. This was checked by doubling the number of points in x and y direction. A typical y grid consists of 200 or 400 points.

The defect-layer equation (7) only depends on the single coordinate η. This ordinary differential equation was numerically discretized with a second-order difference scheme, applying 200 or 400 points. An iteration process was used to satisfy the boundary conditions and the integral restriction.

4. Direct numerical simulations

DNS were carried out for the pressure gradients $\beta \approx 0.25$ and $\beta \approx 0.65$ with a code developed at KTH and FFA by Lundbladh *et al.* (1992, 1994). The spectral method applies Fourier modes in the horizontal directions and Chebyshev modes in the wall-normal direction. Since the boundary layer is developing in the downstream direction, the physical boundary conditions in that direction are non-periodic. To capture these with periodic Fourier modes, a fringe region is added downstream of the physical domain, where the flow is forced from the outflow of the physical domain to the inflow. In this way the physical domain and the fringe region together satisfy periodic boundary conditions. The fringe region is implemented by the addition of a volume force having a form designed to minimize the upstream influence. Time integration is performed using a third-order Runge-Kutta method for the advective and forcing terms and Crank-Nicolson for the viscous terms.

The simulations start with a laminar boundary layer at the inflow which is tripped by a random volume force near the wall. All the quantities are nondimensionalized by the free-stream velocity and the displacement thickness at the starting position of the simulation ($x = 0$) where the flow is laminar. At that position $Re_{\delta^*} = 400$. The length (including the fringe), height and width of the computational domain were $450 \times 24 \times 24$ δ^* units.

The number of modes was $480 \times 161 \times 96$, which gives a resolution in plus units of $\Delta x^+ = 16$ and $\Delta z^+ = 4.3$. The useful region was confined to

$x^* = x/\delta^* = 150 - 350$ which corresponds to Re_{δ^*} from 550 to 1200 or Re_θ from 330 to 700. The simulations were run for a total of 4500 time units (δ^*/U), and the sampling for the turbulent statistics was performed during the 2000 last time units. The good accuracy of the DNS and its statistics was verified by repeating the computation on a coarser resolution ($320 \times 101 \times 64$ modes), and with a shorter averaging time (1000 time units).

5. Large-Re behaviour

The boundary-layer equations were solved for the four turbulence models with different β values. The calculations were started at $Re_\theta = 300$, where the results from DNS by Spalart (1988) for a zero-pressure gradient were used as starting profiles. At each downstream position the outer-edge velocity was iteratively updated until the chosen β was obtained. The calculations were extended up to about $Re_\theta = 10^8$.

For all considered models the classical scalings turn out to appear for increasing Reynolds number. An example is given in Fig. 1, which shows the velocity and Reynolds-shear stress in the inner and outer layer, as obtained with the DRSM for $\beta = 1$. In the inertial sublayer, being the outer part of the inner layer, the velocity (Fig. 1a) converges to the logarithmic law-of-the-wall; the generally accepted best fit to experiments (having $\kappa = 0.41$ and $C = 5$) is shown as a long-dashed line. The velocity in the outer layer (Fig. 1b), when scaled with u_τ and Δ, converges to a single similarity profile, the so-called defect law. Only the solution for $Re_\theta = 10^3$ shows some deviation from the similarity state, but up to at least graphical accuracy no changes are found from $Re_\theta = 10^4$ on. The Reynolds shear stress in the outer part of the inner layer (Fig. 1c) approaches the wall function $-\overline{u'v'}^+ = 1$. The Reynolds shear stress in the outer layer (Fig. 1d) converges to a similarity shape, which shows a local maximum. The appearance of a maximum for the Reynolds shear stress in the outer layer (with $-\overline{u'v'}/u_\tau^2 > 1$), and also for the turbulent kinetic energy, is characteristic for adverse pressure gradient boundary layers ($\beta > 0$); such a maximum is not found for the zero pressure gradient boundary layer ($\beta = 0$). We checked that the similarity profiles for the different quantities in the inner layer are independent of β, which is in agreement with the classical theory, showing that the same wall function holds independent of the pressure gradient.

We verified that the boundary-layer solution in the outer layer converges to the similarity solution described by the defect-layer equation (7). However, the convergence rate for increasing Re_θ towards the similarity state becomes slower for increasing β. For example, for all β values the shape factor converges to $H = 1$ at $Re_\theta \to \infty$, but the shape factor at $Re_\theta = 10^8$ for $\beta = 0$, 8 and 20 still is 14%, 47%, and 71%, respectively, above its asymptotic value.

An interesting practical question is how the outer-edge velocity should be chosen to realize an equilibrium turbulent boundary layer, as represented by a certain constant β value. Bradshaw (1967) has suggested that a practically

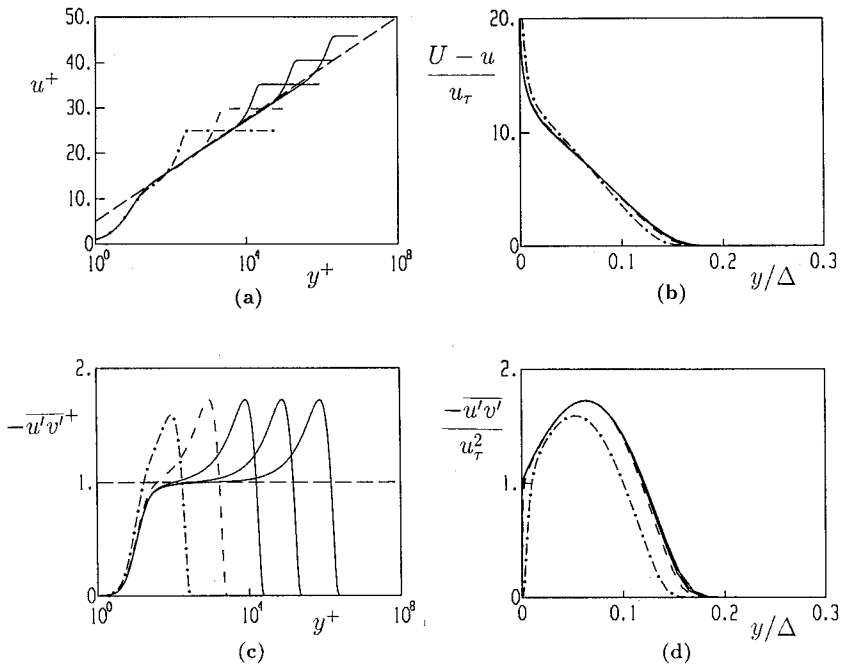

FIGURE 1. Appearance of the law-of-the-wall and the defect law for increasing Reynolds number according to the DRSM with $\beta = 1$; $Re_\theta = 10^3$ $(- \cdot -)$, 10^4 $(- -)$, 10^5, 10^6, and 10^7 (solid lines); Velocity in (a) the inner layer and (b) the outer layer; Reynolds shear stress in (c) the inner layer and (d) the outer layer. (long dash in (a) denotes the experimental wall function for the velocity, and in (c) the theoretical wall function for the Reynolds shear stress).

constant β results if the outer-edge velocity is chosen as $U \propto (x - x_o)^m$ (where x_0 is a virtual origin, and m is a constant power). To verify this we prescribed m and computed β for increasing Re_θ, but β turns out to be very sensitive to m when m comes closer to -0.25 (that is where turbulent separation is about to occur). This problem was overcome by prescribing β instead of m. Fig. 2 shows the results for the DRSM. Here the local m value is defined as $\frac{x}{U}\frac{dU}{dx}$. The turbulence model does not give a Reynolds-number independent m power for equilibrium layers; instead the power becomes slightly more negative for increasing Reynolds number.

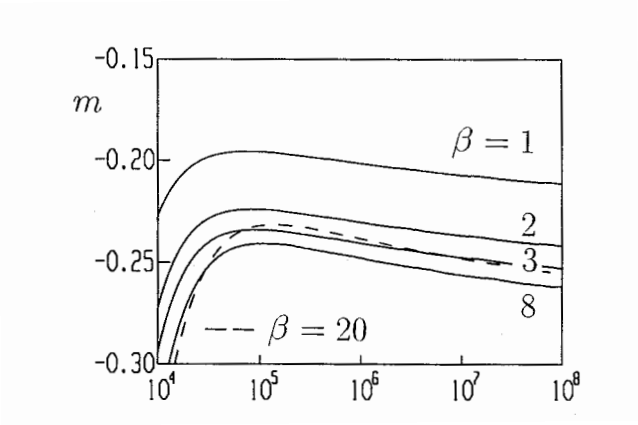

FIGURE 2. Reynolds-number dependence of the m power in the outer-edge velocity according to the DRSM.

Some authors, including Clauser (1954) (who measured $\beta \approx 2$ and 8), have reported difficulties to establish a stable flow in the windtunnel when the adverse pressure gradient becomes stronger. On the grounds of this experience, Clauser has suggested that the same outer-edge velocity (represented by the same m value) can correspond with two equilibrium boundary layers (i.e. two β values). This means that an established experimental equilibrium boundary layer can suddenly lose stability and jump to the other flow type. This is indeed what is found with the DRSM in Fig. 2. For a given Re_θ (above 10^6) the m-power decreases for β values up to about 8, above which the power increases again. For example, the m value for $\beta = 3$ is almost the same as for $\beta = 20$ (for which experiments were performed by Skåre & Krogstad, 1994). A similar nonuniqueness is found with the other turbulence models.

6. Comparison with experiments

The solution in the outer layer, as computed from the boundary-layer equations with different turbulence models, is compared with experiments in Fig. 3 for the streamwise velocity and in Fig. 4 for different turbulence quantities. The computational curves correspond to $Re_\theta = 10^6$ for $\beta = 2$ and 8, and to $Re_\theta = 5 \times 10^4$ for $\beta = 20$. All models, except for the $k - \epsilon$ model, closely predict the experimental streamwise velocity (Fig. 3); the $k - \epsilon$ model overpredicts the experimental wall-shear stress coefficient for $\beta = 20$ at $Re_\theta = 5 \times 10^4$ by 145%. The DRSM is superior, as it gives a value which is only 7% too large, whereas the algebraic model and the $k - \omega$ model give a slightly larger deviation of -15% and $+17\%$, respectively.

All models also closely reproduce the experimental Reynolds-shear stress (Fig. 4a), but the $k - \epsilon$ model somewhat overpredicts the boundary-layer thickness. The DRSM predicts the structure parameter ($= -\overline{u'v'}/k$) best (Fig. 4b), and is in fact very close to the experiments for $\beta = 20$. The DRSM also gives a quite good prediction of the Reynolds normal stresses (Fig. 4c).

With respect to the structure parameter, the experiments in Fig. 4b show that its value is almost constant, and equal to about 0.3, across most of the outer-layer thickness. This implies that the Reynolds shear stress is proportional to the turbulent kinetic energy, as was also discussed by Bradshaw (1967) on the grounds of his own experiments for a weaker adverse pressure gradient. Most turbulence models (including the $k - \epsilon$ model, the $k - \omega$ model, and the DRSM) have chosen the model constants such that the proportionality with the structure parameter 0.3 is reproduced for flows in which the production of turbulence energy P_k ($= -\overline{u'v'}\partial u/\partial y$) equals the turbulent dissipation rate ϵ. For example the $k - \epsilon$ model has $-\overline{u'v'} = \nu_t \partial u/\partial y$, with $\nu_t = c_\mu k^2/\epsilon$. As the constant c_μ is set to 0.09 this gives $-\overline{u'v'}/k = 0.3$ when $P_k = \epsilon$.

7. Comparison with DNS

The DNS were performed for the outer edge velocity $U \propto (x - x_0)^m$, with $m = -0.077$ and $m = -0.15$. At the relatively low Re_θ up to which the DNS were feasible, the corresponding equilibrium parameter β is found to be about 0.25 and 0.65, and the shape factor H is about 1.60 and 1.63, respectively.

The calculations with the DRSM at low Reynolds numbers are compared with the new DNS. Profiles for the velocity and turbulence obtained from the DNS at $x^* = 150$ were used as initial data for the model calculations. We varied the initial turbulence and dissipation rate in the model computations, and found that the initial transients already had decayed at $x^* = 335$, where the comparison with the DNS was made. Thus the comparison is meaningful since the difference between the model predictions at low and high Reynolds number (see Fig. 5) are due to the dependence on the Reynolds number and not to the influence of the initial conditions.

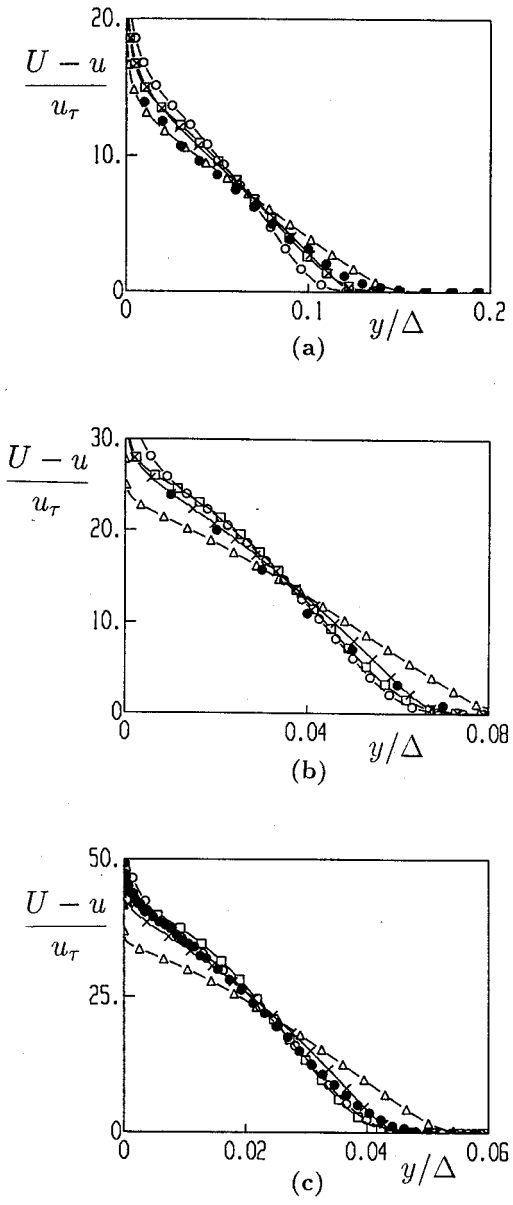

FIGURE 3. Comparison between turbulence models and experiments for the streamwise velocity under different equilibrium conditions; (a) $\beta = 2$ (• experiments by Clauser), (b) $\beta = 8$ (• experiments by Clauser), (c) $\beta = 20$ (• experiments by Skåre and Krogstad), models: O−O algebraic; $\triangle - \triangle$ $k-\epsilon$; $\times - \times$ $k-\omega$; $\square - \square$ DRSM

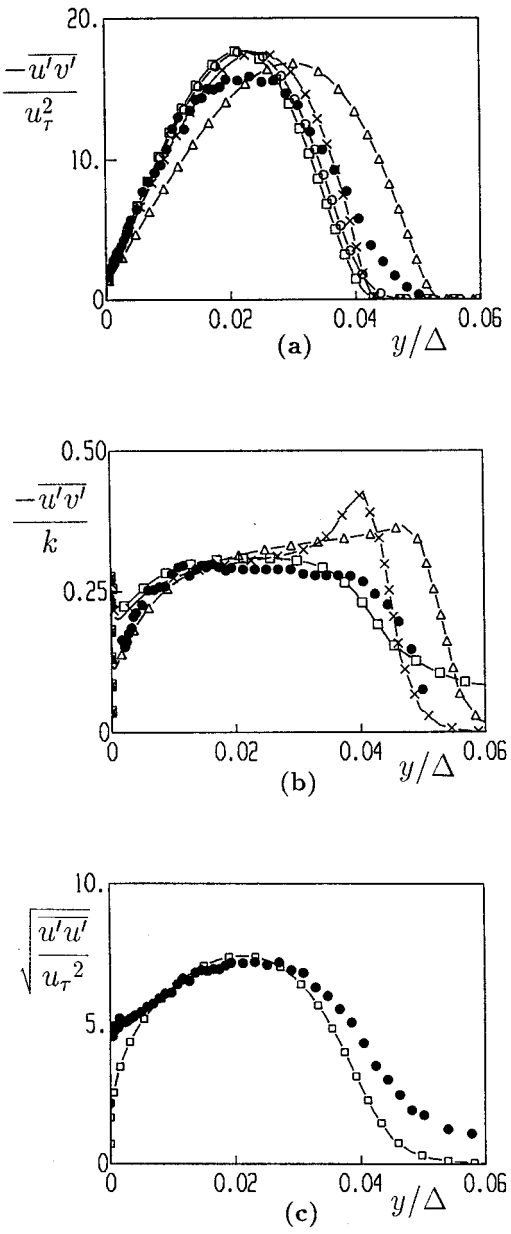

FIGURE 4. Comparison between turbulence models and experiments for the turbulence in an equilibrium boundary layer with $\beta = 20$; (a) Reynolds shear stress, (b) structure parameter, (c) Reynolds normal stress along the wall. models: O−O algebraic; $\triangle - \triangle$ $k-\epsilon$; $\times - \times$ $k-\omega$; $\square - \square$ DRSM

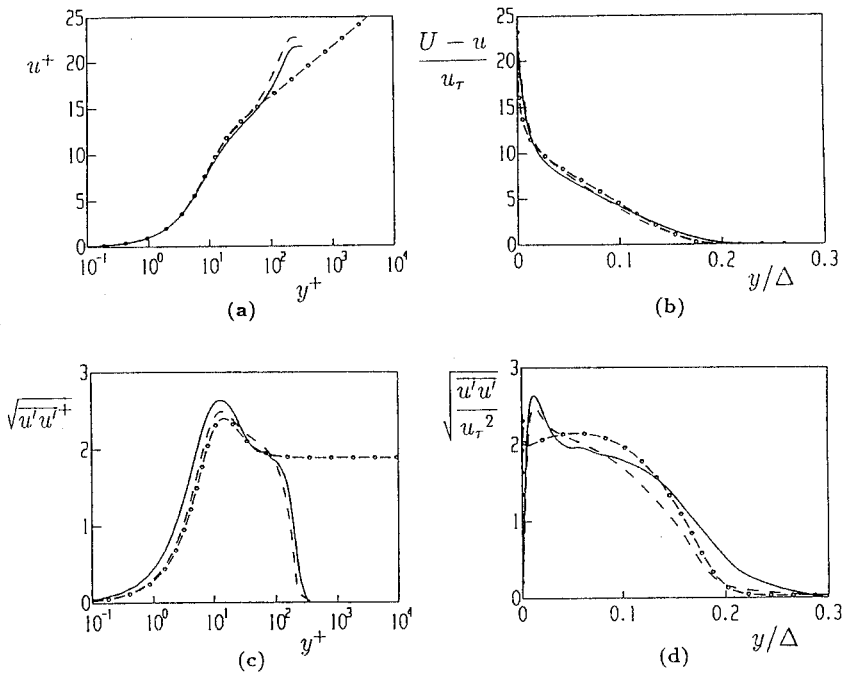

FIGURE 5. Comparison for $\beta \approx 0.65$; — DNS at $Re_\theta = 670$; - - DRSM at $Re_\theta = 670$; -o- similarity solution for the DRSM. Streamwise velocity in (a) inner-layer scalings, and (b) outer-layer scalings. Streamwise normal stress in (c) inner-layer scalings and (d) outer-layer scalings.

Figs 5a,b show close agreement for the velocity profile in inner-layer and outer-layer scalings at $Re_\theta = 670$ and $\beta \approx 0.65$, as computed with the DNS and DRSM. The figure also shows the large-Re similarity state for the DRSM. In fact $Re_\theta = 670$ is still so low that only a small logarithmic part in the inner layer is found. The streamwise Reynolds normal stress for $\beta \approx 0.65$ is compared in Figs 5c,d. The results are shown in both inner and outer layer scalings, and the similarity solution for the DRSM is included as well. Differences between the solution at $Re_\theta = 670$ and the similarity solution are significant. The results with the DRSM closely agree with the DNS at $Re_\theta = 670$, showing that the DRSM reproduces the physics of adverse pressure-gradient boundary layers at relatively low Reynolds numbers. The peak in the Reynolds normal stress in the DNS and DRSM at $Re_\theta = 670$ is part of the inner layer, but there already is a tendency to develop a second peak in the outer layer, which indeed has been established in the similarity solution with the DRSM. New DNS at larger

β, which will show an even stronger peak in the outer layer for the turbulent kinetic energy, are underway.

8. Conclusions

The numerical solution of the boundary-layer equations up to $Re_\theta = 10^8$ shows that four classes of turbulence models converge to the same classical scalings in the inner and outer layer for turbulent equilibrium boundary layers under an adverse pressure gradient. The solution in the outer layer converges to the defect law described by the defect-layer equation of Tennekes & Lumley, and not to the defect-layer equation of Wilcox (only for $\beta = 0$, both formulations are equal). Convergence to the similarity solution becomes slower for increasing β value. There is a nonunique relation between the m power in the outer-edge velocity and the equilibrium parameter β for all four turbulence models, which is in agreement with the experimental findings of Clauser.

Comparison with experiments, particularly the recent experiments by Skåre and Krogstad at $\beta = 20$, shows that among the tested turbulence models, the Differential Reynolds Stress Model is superior. But also the algebraic model and the $k-\omega$ model are reasonably accurate. The $k-\epsilon$ model gives rather large deviations for strong adverse pressure gradients, where it considerably overpredicts the wall-shear stress. The DRSM was also compared with our new DNS for $\beta \approx 0.25$ and 0.65 at the relatively low Reynolds number $Re_\theta = 670$. It turns out that the DRSM correctly predicts the low-Reynolds-number effects for the evolution of the boundary layer to its high-Re similarity solution.

References

Bradshaw, P. 1967 The turbulent structure of equilibrium boundary layers. *J. Fluid Mech.* **29**, 625–645.

Cebeci, T. & Smith, A. M. O. 1974 *Analysis of Turbulent Boundary Layers*. Academic Press.

Clauser, F. H. 1954 Turbulent boundary layers in adverse pressure gradients. *J. Aero. Sci.* **21**, 91–108.

Coles, D. 1956 The law of the wake in the turbulent boundary layer. *J. Fluid Mech.* **1**, 191–226.

Hanjalić, K., Jakirlić, S. & Hadžić, I. 1995 Computation of oscillating turbulent flows at transitional *Re*-numbers. In *Turbulent Shear Flows 9* (eds. F. Durst, N. Kasagi & B. E. Launder), pp. 323–342. Springer-Verlag.

Henkes, R. A. W. M. 1997 Comparison of turbulence models for attached boundary layers relevant to aeronautics. *Appl. Sci. Res.* **57**, 43–65.

Henkes, R. A. W. M. 1998 Scaling of equilibrium boundary layers under adverse pressure gradient using turbulence models. *AIAA J.* **36**, 320–326.

Launder, B. E. & Sharma, B. I. 1974 Application of the energy-dissipation model of turbulence to the calculation of flow near a spinning disk. *Let. Heat Mass Transfer* **1**, 131 – 138.

Lundbladh, A., Henningson, D. S. & Johansson, A. V. 1992 An efficient spectral integration method for the solution of the Navier-Stokes equations. FFA-TN 1992-28, Aeronautical Research Institute of Sweden, Bromma.

Lundbladh, A., Schmid, P. J., Berlin, S. & Henningson, D. S. 1994 Simulation of bypass transition in spatially evolving flows. Proceedings of the AGARD Symposium on Application of Direct and Large Eddy Simulation to Transition and Turbulence, AGARD-CP-551.

Skåre, P. E. 1994 Experimental investigation of an equilibrium boundary layer in strong adverse pressure gradient. University of Trondheim, PhD Thesis, Report NTH 1994:179 (D).

Skåre, P. E. & Krogstad, P.-Å. 1994 A turbulent equilibrium boundary layer near separation. *J. Fluid Mech.* **272**, 319–348.

Spalart, P. R. 1988 Direct simulation of a turbulent boundary layer up to $Re_\theta = 1410$. *J. Fluid Mech.* **187**, 61–98.

Tennekes, H. & Lumley, J. L. 1972 *A First Course in Turbulence*. The MIT Press.

Wilcox, D. C. 1993 *Turbulence Modeling for CFD*. DCW Industries, Inc.